Journal of Materials Chemistry C

ROYAL SOCIETY OF CHEMISTRY

PAPER

View Article Online
View Journal

Cite this: DOI: 10.1039/d4tc02477j

Ultra-stable $CsPbBr_3$-embedded polymer films for spectrally tunable X-ray nuclear batteries and flexible radiation imaging applications†

Dongdong Liang,[a] Zhiheng Xu, *[ab] Dandan Yang, *[c] Zhibin Xu,[a] Weitong Yin[a] and Xiaobin Tang*[ab]

Received 13th June 2024,
Accepted 9th September 2024

DOI: 10.1039/d4tc02477j

rsc.li/materials-c

Luminescence instability in service environments has limited the widespread use of halide perovskite materials, especially for X-ray energy conversion and detection/imaging. This work proposed a method for improving luminescence stability through polymer encapsulation, which is more convenient than compositional engineering and surface modulation. Meanwhile, the differences in the luminescence intensities of composite films synthesized by encapsulation of different polymer matrices and their luminescence stability under various harsh X-ray irradiation conditions were systematically investigated. The applications of the developed $CsPbBr_3$-embedded polymer films with excellent luminescence performance and high service stability in X-ray radiation energy utilization and detection/imaging were discussed. The results show that $CsPbBr_3$-embedded PS films can meet the spectral modulation requirements of radioluminescent materials for nuclear batteries and can also fulfill the needs of flexible X-ray imaging with a high spatial resolution.

1. Introduction

X-rays, which are electromagnetic waves with extremely high frequency, short wavelength, and high energy, play an important role in the fields of medical diagnosis, industrial flaw detection, safety inspection, and energy conversion.[1–4] In recent years, X-rays have been widely used in nuclear battery performance analysis and radiation detection/imaging due to their high energy and strong penetration characteristics.[5–8] Radioluminescent (RL) materials, which can convert high-energy photons of X-rays into low-energy photons, thereby realizing energy conversion and facilitating detection, play a crucial role in X-ray nuclear batteries and radiation imaging.[9–14] However, conventional high performance inorganic fluorescent materials, such as CsI:Tl, NaI:Tl, BGO, and LYSO, usually find it difficult to regulate luminescence and require high-temperature calcination and synthesis and it is difficult to prepare these materials with a large area and flexibility, thus limiting their applications.[15–19] Halide perovskites have attracted significant research interest due to their solution-based synthesis, tunable emission spectra, and high luminescence efficiency, thus providing an economical and convenient option for X-ray energy conversion and imaging.[20–27]

The stability problems of halide perovskites seriously hinder their performance in practical applications, despite their excellent optical properties.[28–31] Wang *et al.* proposed that introducing FA at the A site of the halide perovskite structure could stabilize the nanocrystals.[32] Tan *et al.* reported that replacing OA/OLA ligands with octylphosphonic acid (OPA) dramatically improves the stability of $CsPbX_3$.[33] Wang *et al.* demonstrated that trioctylphosphine can effectively recover the luminescence emission of aged inorganic lead halide perovskite quantum dots and improve their long-term storage stability.[34] Yang *et al.* reported an armor-like passivation strategy to enhance the comprehensive stability of $CsPbBr_3$ quantum dots.[35] Unfortunately, such compositional engineering and surface modulation methods are limited by the complexity of ion doping and ligand selection.[36] Recently, the polymer matrix encapsulation strategy has been demonstrated to be an effective and convenient method to improve the luminescence stability of halide perovskites.[37–40] Liu *et al.* prepared a perovskite–polymer composite luminescent elastomer with excellent stability against all harsh aqueous environments.[41] Teng *et al.* reported a PDCPD@PNC composite luminescent material, which exhibited long-term stability in water

[a] Department of Nuclear Science and Technology, Nanjing University of Aeronautics and Astronautics, Nanjing 211106, China. E-mail: xuzhiheng@nuaa.edu.cn, tangxiaobin@nuaa.edu.cn
[b] Key Laboratory of Nuclear Technology Application and Radiation Protection in Aerospace, Ministry of Industry and Information Technology, Nanjing 211106, China
[c] Institute of Innovation Materials and Energy, School of Chemistry and Chemical Engineering, Yangzhou University, Yangzhou, 225002, China. E-mail: dandanyang@yzu.edu.cn

† Electronic supplementary information (ESI) available. See DOI: https://doi.org/10.1039/d4tc02477j

and strongly acidic and alkaline solutions.[42] However, research on matrix encapsulation to enhance the stability of halide perovskites is relatively limited and mainly focuses on improving the luminescent stability of perovskites in aqueous environments. The improvement in the luminescence stability of composite films under harsh X-ray irradiation conditions and at high and low temperatures is still not reported, which poses a challenge for the use of halide perovskite-embedded polymer films in X-ray energy conversion and imaging applications.

In this work, we have investigated the luminescence stability of $CsPbBr_3$-embedded polymer films from multiple perspectives. In particular, $CsPbBr_3$-embedded polystyrene films exhibit excellent luminescence stability under irradiation, at high and low temperatures, and in aqueous environments; they can still retain 79.15% of RL intensity under equivalent continuous irradiation for 10 years, show very small fluctuations in RL intensity at a 100 K temperature difference (233–333 K), and exhibit long-term stability in the water environment. Meanwhile, the proposed thin-film preparation scheme has strong competitive advantages of achieving a wide wavelength range adjustment and good radiation imaging characteristics, which are suitable for X-ray energy conversion for power generation and detection analysis.

2. Materials and methods

2.1 Materials

Cesium acetate (CsAc, AR, 99%), lead bromide ($PbBr_2$, AR, 99%), lead chloride ($PbCl_2$, AR, 99.5%), lead iodide (PbI_2, 98%), and the ethylene-vinyl acetate (EVA) copolymer were purchased from Macklin. Propanol (1-PrOH, AR, 99%), *n*-hexane (Hex, AR, 97%), *n*-octanoic acid (OcAc, AR, 99%), *n*-octylamine (OcAm, AR, 99%), polystyrene (PS), and polymethyl methacrylate (PMMA) were purchased from Aladdin. Polydimethylsiloxane (PDMS) was purchased from Dow Corning. Toluene (TOL) was purchased from Nanjing Reagent. All chemicals were used without any further purification.

2.2 Synthesis of $CsPbBr_3$ nanowires

Firstly, the Cs precursor and the $PbBr_2$ precursor were synthesized. The Cs precursor solution was synthesized by dissolving 128 mg of CsAc in a mixed solution containing 12 mL of 1-PrOH and 24 mL of hexane under stirring at room temperature. The $PbBr_2$ precursor solution was prepared by dissolving 980 mg of $PbBr_2$ in a mixed solution containing 1.8 mL of 1-PrOH, 1.8 mL of OcAc, and 1.8 mL of OcAm under vigorous stirring at 90 °C. Then, the hot $PbBr_2$ precursor solution was quickly injected into the Cs precursor solution, and the solution turned green within a few seconds. Finally, the $CsPbBr_3$ nanowires (NWs) were obtained by centrifuging at 4000 rpm for 3 min.

2.3 Preparation of $CsPbBr_3$-embedded polymer films

A typical preparation procedure was carried out according to the following steps: firstly, $CsPbBr_3$ NWs (100 mg) and the polymer (1 g) were dissolved in 4 mL of toluene under stirring. Subsequently, the uniform mixed solution was spin-coated onto a quartz glass substrate at 600 rpm for 60 s. Thirdly, the samples were cured at 45 °C for 6 hours in a vacuum environment. Finally, the films were easily obtained by separating them from the glass base.

2.4 Anion exchange reaction

$CsPbBr_3$ NWs (60 mg) were firstly dispersed in 1.2 mL of toluene before exchanging Br^- anions with Cl^- or I^-. Then, 50–300 μL of $PbCl_2$ or PbI_2 precursor solution (137 mg mL^{-1} or 230 mg mL^{-1} $PbCl_2$ or PbI_2 dissolved in a mixed solution of 1-PrOH, OcAc, and OcAm with the same volume ratio) were directly added to the $CsPbBr_3$ NW solution. The synthesis method is the same as that of the $PbBr_2$ precursor solution. After anion exchange reaction, $CsPbBr_{3-x}Cl_x$ or $CsPbBr_{3-x}I_x$ was obtained by centrifuging the solution multiple times.

2.5 Measurements and characterization

X-ray diffraction was performed using an Empyrean X-ray diffractometer. PL and RL spectra of $CsPbBr_3$ NWs and $CsPbBr_3$-embedded polymer films were acquired using an Agilent Cary Eclipse spectrometer. SEM images were obtained by using a LYRA3 GMU scanning electron microscope. The XPS test was performed on an ESCALAB Xi +. Temperature-dependent photoluminescence spectra of these films were measured using an FLS1000 spectrometer. The long-term equivalent irradiation experiment was conducted at the irradiation centre of the Nanjing University of Aeronautics and Astronautics. The electrical properties of the radioluminescent nuclear batteries were evaluated using the Keithley 2636A source meter. X-ray energy spectra were obtained using the HPGe detector (ORTEC GL0110P). X-ray imaging images were obtained by using an electron-multiplying charge-coupled device (EMCCD) camera (Andor iXon Ultra 888) equipped with a Canon EF 24–70 mm f/2.8L II USM zoom lens. ImageJ was used to analyze the quality of X-ray imaging images.

3. Results and discussion

3.1 Characterization of $CsPbBr_3$-embedded polymer films

The $CsPbBr_3$ NWs were synthesized *via* a modified co-precipitation method and can be obtained by single-step injection at room temperature.[43,44] The preparation process of $CsPbBr_3$-embedded polymer films is shown in Fig. 1a. Compared to the solution, the thin-films of RL materials are more competitive due to the absence of the layered aggregation phenomenon (Fig. S1, ESI†). However, the directly prepared $CsPbBr_3$ NW film is not suitable for practical X-ray applications, as the unevenness of the film surface seriously affects the uniformity of luminescence (Fig. S2, ESI†). At the same time, the film is very unstable in the water environment and generally loses its luminescence after being immersed in the water environment for about 1.5 hours (Fig. S3, ESI†). To solve the problem mentioned above, we selected four kinds of polymers to embed $CsPbBr_3$ NWs (Fig. 1b), such as polystyrene (PS), polymethyl methacrylate (PMMA), polydimethylsiloxane (PDMS), and the ethylene-vinyl acetate (EVA) copolymer, as shown in Fig. S4 (ESI†). Briefly, both the prepared $CsPbBr_3$

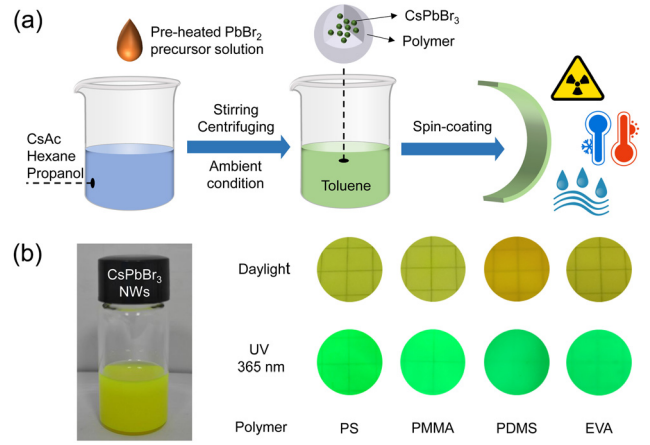

Fig. 1 (a) Schematic of the synthetic process of $CsPbBr_3$ NWs embedded in polymer films stabilized under radiation and in hot, cold, and aqueous environments. (b) Physical morphology image of $CsPbBr_3$ NWs and $CsPbBr_3$-embedded polymer films under daylight and 365 nm UV excitation.

nanowires and high chemically inert and transparent polymer were mixed and dissolved in toluene to form a homogeneous solution. Then, the mixture was spin coated on a quartz substrate followed by thermal annealing at 40 °C for 10 min, resulting in uniform and transparent composite films.

As shown in Fig. 2a and b, the microscopic morphology images of $CsPbBr_3$ NWs and $CsPbBr_3$-embedded PS films show good linearity and homogeneity, respectively, and the NWs are well-coated with the polymer without the agglomeration phenomenon. In terms of luminescence, all of these films emit green light under UV and X-ray radiation. Interestingly, the $CsPbBr_3$-embedded PS film has the highest luminescence intensity when the amount of materials is the same (Fig. 2c and d). As shown in Fig. 2e, all $CsPbBr_3$-embedded polymer films show the characteristic diffraction peaks of $CsPbBr_3$ NWs at two theta values of 21.5° (010) and 30.5° (210), which indicate that the proposed polymer matrix encapsulation strategy does not completely destroy the structure of $CsPbBr_3$ NWs.

However, the PDMS-based film shows the lowest intensity of diffraction peaks for $CsPbBr_3$ NWs among the four types of polymer-based films, which is due to the weakened crystallization of perovskite nanowires in the PDMS-based film relative to other polymers. Meanwhile, the UV-visible absorption test indicates that the EVA-based film, similar to the PDMS-based film, does not show obvious characteristic absorption of $CsPbBr_3$ NWs (Fig. 2f). We attribute this finding to the fact that such water-based polar polymers can destroy the crystal structure of the perovskite, thus leading to low luminescence when exposed to UV or X-ray excitation.[45,46]

To further investigate the intrinsic reasons for the excellent optical properties of $CsPbBr_3$-embedded PS films, we explored the interaction between the polymer and the perovskite in the composite films. X-ray photoelectron spectra (XPS) and temperature-dependent photoluminescence spectra were recorded. Fig. 3a shows the chemical state of Pb in the four samples. The $CsPbBr_3$-embedded PS and EVA films show Pb 4f peaks at 144.0 eV and 139.0 eV, respectively, showing a movement to a

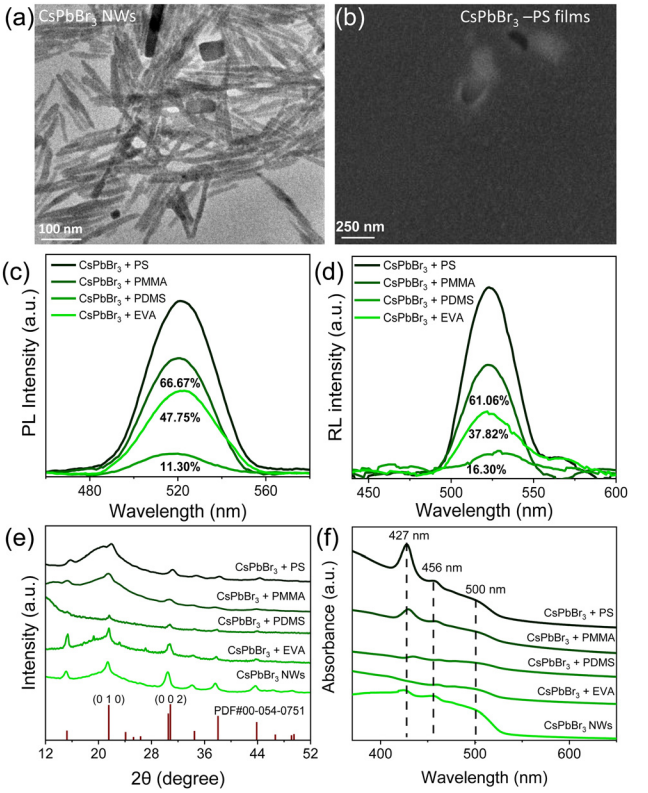

Fig. 2 Microscopic morphology images of (a) $CsPbBr_3$ NWs and (b) $CsPbBr_3$-embedded PS films. (c) Photoluminescence and (d) radioluminescence spectra of $CsPbBr_3$-embedded polymer films. (e) XRD patterns of $CsPbBr_3$-embedded polymer films and $CsPbBr_3$ NWs. (f) Absorption spectra of $CsPbBr_3$-embedded polymer films and $CsPbBr_3$ NWs.

high binding energy of 1.1 eV compared with $CsPbBr_3$ NWs, which is attributed to the fact that the electron absorption capacity of Pb is less than that of O and the benzene ring, and the electron cloud density around Pb decreases and shifts to high binding energy. Similarly, the Pb 4f peaks of the $CsPbBr_3$-embedded PMMA film shift to a higher binding energy of 0.55 eV. Such coordination interaction can effectively improve stability.[47] However, for $CsPbBr_3$-embedded PDMS films, there is obviously no Pb 4f peak signal, which may be because the lead atom is difficult to coordinate with PDMS molecules (Fig. S4, ESI†). Fig. 3b shows that the PL intensity of $CsPbBr_3$-embedded

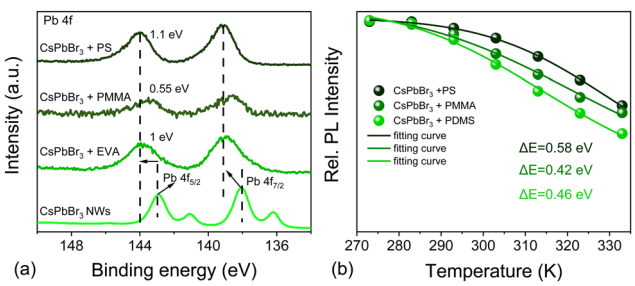

Fig. 3 (a) XPS spectra of Pb 4f of $CsPbBr_3$-embedded polymer films and $CsPbBr_3$ NWs. (b) Relationship between photoluminescence intensity and temperature for different $CsPbBr_3$-embedded polymer films.

PS, PMMA and PDMS films starts to decrease with the increase of temperature from 273 K to 333 K. According to the Arrhenius equation (eqn (1)), where I_0 represents the PL intensity at 273 K, A is a constant, and k_B is the Boltzmann constant, the calculated activation energies (ΔE) of these films are 0.58 eV, 0.42 eV, and 0.46 eV, respectively. The higher activation energy of the $CsPbBr_3$-embedded PS film means a small proportion of thermally activated non-radiative recombination, ensuring the high luminescence performance of $CsPbBr_3$ NWs.[48] However, for $CsPbBr_3$ NWs and the embedded EVA film, the PL intensity decreases continuously with the increase of temperature from 233 K to 333 K, indicating the low thermal stability (Fig. S5 and S6, ESI†).

$$\frac{I(T)}{I_0} = \frac{1}{1 + A\exp\left(-\frac{\Delta E}{k_B T}\right)} \quad (1)$$

3.2 Luminescence stability of $CsPbBr_3$-embedded polymer films

The luminescence stability of $CsPbBr_3$-embedded polymer films is an important factor to consider in the field of X-ray imaging. Here, we investigated the stability differences of $CsPbBr_3$-embedded polymer films from multiple perspectives, including irradiation, high and low temperatures, and aqueous environments. As shown in Fig. 4a, $CsPbBr_3$-embedded polymer films exhibit good luminescence stability, even after continuous irradiation with 5.639 μGy s^{-1} X-rays for 1 hour; there are no significant changes in luminescence intensity. On this basis, we established a long-term irradiation equivalence experiment to further investigate the difference in the luminescence stability of $CsPbBr_3$-embedded polymer films under large cumulative irradiation. As shown in Fig. 4b, the PS-based film exhibits excellent radio stability, retaining 79.15% of RL intensity under equivalent continuous irradiation for 10 years. In view of the excellent radiation resistance of the PS polymer matrix, when the perovskite matrix is exposed to irradiation, the irradiation damage effect can be effectively reduced. The thermal quenching effect inherent in the $CsPbBr_3$ perovskite will affect its performance in X-ray applications.[49,50] Compared to the bare $CsPbBr_3$ NWs, embedding $CsPbBr_3$ with polymers can reduce the influence of temperature on their luminescence intensity (Fig. S5 and S6, ESI†). In particular, the luminescence intensity of the $CsPbBr_3$-embedded PS film is the least affected, and it can retain over 51.62% of the maximum luminescence intensity at 333 K. In addition, as mentioned above, $CsPbBr_3$ NWs are prone to losing luminescent properties in aqueous environments, and thus here we also explored the luminescence stability of $CsPbBr_3$-embedded polymer films. As shown in Fig. 4c and d, compared to the brittleness of the PMMA-based film, the hydrophilicity of the EVA-based film, and the poor luminescence intensity of the PDMS-based film, the $CsPbBr_3$-embedded PS film has better luminescence intensity and stability, and it can retain over 84.72% of the initial luminescence intensity after immersion in water for 66 days, and its luminescence stability is better than the reported 15 day decay to 85% in the literature.[51] Obviously, the excellent stability of $CsPbBr_3$-embedded PS films can be attributed to

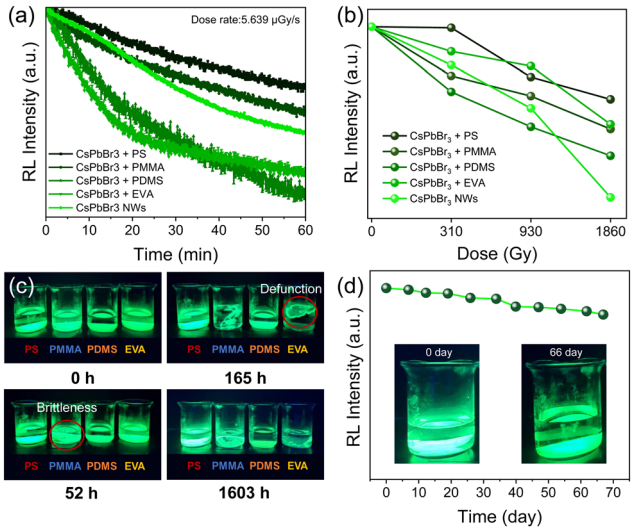

Fig. 4 (a) RL intensity of $CsPbBr_3$-embedded polymer films upon exposure to X-ray radiation at 5.639 μGy s^{-1} for 1 h. (b) Degradation of RL intensity of $CsPbBr_3$-embedded polymer films under irradiation. (c) Variation in photoluminescence of $CsPbBr_3$-embedded polymer films in water under 365 nm excitation. (d) RL intensity evolution of $CsPbBr_3$-embedded PS films in water over 66 days.

the good physical shielding effect of the PS polymer, which prevents the intrusion of moisture from destroying their structural integrity. Accordingly, $CsPbBr_3$-embedded PS films exhibit stronger competitive advantages of excellent luminescence intensity and stability, when in long-term service under harsh irradiation conditions and in the water environment.

3.3 Application of $CsPbBr_3$-embedded PS films in radioluminescent nuclear batteries

We further explored the applications of the developed $CsPbBr_3$-embedded PS films in X-ray absorption and utilization. Radioluminescent nuclear batteries are an important form of X-ray energy conversion and utilization technology, and their working mechanism is shown in Fig. 5a. Briefly, X-ray energy is first converted into light energy by the fluorescent layer, and then the light energy is converted into electrical output by the photovoltaic module.[52,53] The fluorescent layer plays a bridging role, and their luminescence and stability performance directly determine the overall service performance of the battery. AlGaInP photovoltaic module based nuclear batteries were tested for electrical output performance under X-ray excitation.

As shown in Fig. S7 (ESI†) and Fig. 5b, with the increase of the radiation dose rate, the radioluminescence intensity of $CsPbBr_3$-embedded PS films enhanced, thereby improving the electrical output of the battery. In addition, from the working mechanism of radioluminescent nuclear batteries, it is found that the electrical output is also influenced by the matching degree between the radioluminescence spectra of the fluorescent material and the response range of photovoltaic modules. Compared to conventional fluorescent materials with a fixed bandwidth, $CsPbBr_3$ NWs have the ability to exhibit tunable emission colors and can achieve efficient coupling between the

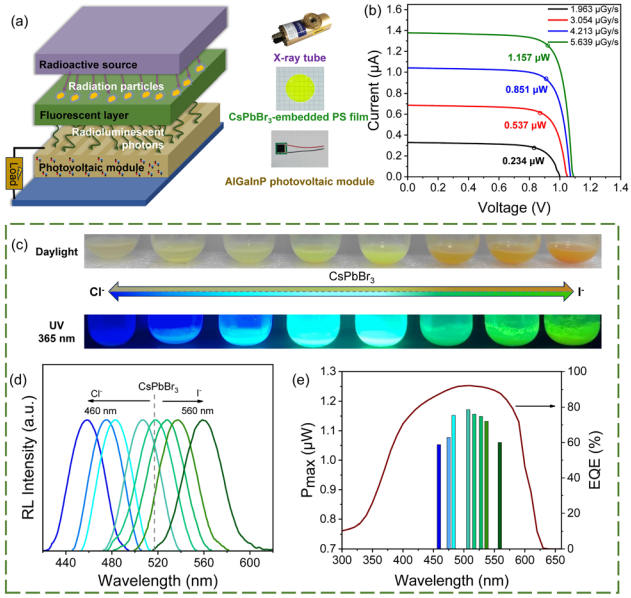

Fig. 5 (a) Schematic illustration of a radioluminescent nuclear battery. (b) *I*–*V* curves and the electrical output of a radioluminescent nuclear battery upon exposure to different X-ray radiation sources. (c) Photography of anion exchange samples with Cl^- or I^- under 365 nm excitation. (d) RL spectra of anion exchange samples with Cl^- or I^-. (e) Variation of the maximum output power of the battery based on different anion exchange sample films over the response interval of the AlGaInP photovoltaic module.

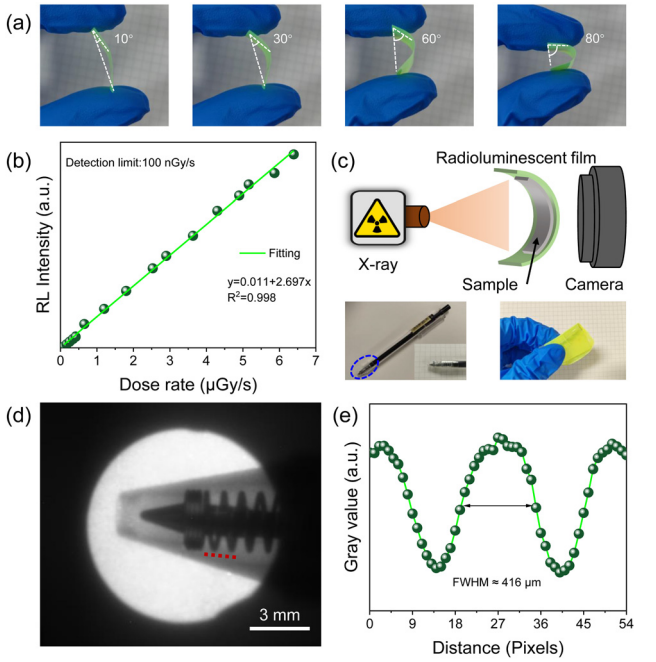

Fig. 6 (a) The multi-angle bending flexibility of $CsPbBr_3$-embedded PS films. (b) Dose rate dependence of the RL intensity of $CsPbBr_3$-embedded PS films. (c) Schematic diagram of flexible X-ray imaging with $CsPbBr_3$-embedded PS films. The bottom panels show the imaging object selected (pen) for the experiment. (d) Photography of the pen after X-ray exposure with $CsPbBr_3$-embedded PS films. (e) Spatial resolution measurement of X-ray imaging along the red line in panel (d).

radioluminescence spectra and the response range of photovoltaic modules. As shown in Fig. 5c–e, we use an anion exchange method to achieve controllable adjustment of the radioluminescence range of $CsPbBr_3$ NWs, which can more closely match the response range of the AlGaInP photovoltaic module. The electrical test results indicate that reasonable control of the radioluminescence spectra range of the fluorescent material can improve the output performance, and the maximum power of the battery can reach 1.172 μW, with an energy conversion efficiency of 0.0898%, which is higher than the reported 0.023% (see the ESI† for further details of energy conversion efficiency calculation).[54] This method is very favorable for effectively solving the long-standing dilemma of low energy conversion efficiency of batteries.

3.4 Application of $CsPbBr_3$-embedded PS films in radiation imaging

Given the excellent flexibility of $CsPbBr_3$-embedded PS films with strong luminescence and high stability, the potential for their application in flexible X-ray imaging was further explored (Fig. 6a). The dose response analysis of a radioluminescent material is crucial in X-ray imaging, which is a technique that uses the dose dependence of RL intensity to generate phase contrast images.[55] As shown in Fig. 6b, the proposed $CsPbBr_3$-embedded PS films exhibit good dose response, with an X-ray response threshold dose rate of 100 nGy s^{-1}, which is lower than that required for conventional computed tomography (5.5 μGy s^{-1}).[56]

A pen was selected as the imaging object to conduct a proof-of-concept imaging experiment (Fig. 6c). The internal contour of the pen can be clearly observed in Fig. 6d. In order to quantitatively evaluate the imaging quality, the point spread function of the intensity profile (the red line in Fig. 6d) was analyzed. The $CsPbBr_3$-embedded PS film could give a clear resolution for the pins of the pen with a FWHM of 416 μm (Fig. 6e), which is better than the reported 504 μm in the literature.[48] The $CsPbBr_3$-embedded PS film can lay a good foundation for high-resolution flexible X-ray imaging in the fields of oral cavity, security check, and explosion detection.

4. Conclusions

In conclusion, $CsPbBr_3$-embedded polymer films with ultra-stability in various environments for applications in X-ray nuclear batteries and radiation imaging have been realized. Through investigating the luminescence stability differences of $CsPbBr_3$-embedded polymer films from multiple perspectives, we found that $CsPbBr_3$-embedded PS films exhibit excellent luminescence stability; they can still retain 79.15% of RL intensity under 10-year equivalent continuous irradiation conditions, exhibit over 51.62% of the maximum luminescence intensity at 333 K, and retain 84.72% of the initial RL intensity under water for 66 days. Moreover, the proposed $CsPbBr_3$-embedded PS film exhibits tunable emission colors and flexibility and can meet the spectral regulation requirements of

luminescent materials in radioluminescent nuclear batteries and the requirements of flexible X-ray imaging. Based on this, a nuclear battery and an X-ray imaging platform were constructed to demonstrate the application potential of $CsPbBr_3$-embedded PS films in X-ray energy conversion and imaging. This work provides an idea to solve the problems of weak radioluminescence intensity and poor luminescence stability of metal halide perovskite materials, which provide technical support for the development of long-life nuclear batteries and flexible X-ray imaging systems.

Author contributions

Dongdong Liang: conceptualization, investigation, methodology, writing – original draft, writing – reviewing and editing; Zhiheng Xu: validation, data curation, writing – reviewing and editing, funding acquisition, supervision; Dandan Yang: validation, data curation, writing – reviewing and editing; Zhibin Xu: investigation, methodology; Weitong Yin: investigation; and Xiaobin Tang: writing – reviewing and editing, supervision, project administration.

Data availability

The data that support the findings of this study are available from the corresponding author upon reasonable request.

Conflicts of interest

There are no conflicts to declare.

Acknowledgements

We gratefully acknowledge the financial support from the National Natural Science Foundation of China (Grant No. 12005101 and 62204215), the Fundamental Research Funds for the Central Universities (Grant No. NT2023013), and the Postgraduate Research & Practice Innovation Program of NUAA (Grant No. xcxjh20230610).

Notes and references

1 L. Lu, M. Sun, Q. Lu, T. Wu and B. Huang, *Nano Energy*, 2021, **79**, 105437.
2 H. Meng, W. Zhu, Z. Zhou, R. Zhou, D. Yan, Q. Zhao and S. Liu, *J. Mater. Chem. C*, 2022, **10**, 12286–12291.
3 X. Ou, X. Qin, B. Huang, J. Zan, Q. Wu, Z. Hong, L. Xie, H. Bian, Z. Yi, X. Chen, Y. Wu, X. Song, J. Li, Q. Chen, H. Yang and X. Liu, *Nature*, 2021, **590**, 410–415.
4 H. Wu, Y. Ge, G. Niu and J. Tang, *Matter*, 2021, **4**, 144–163.
5 Y. Wu, Z. Xu, Y. Liu, T. Jiang, H. San and X. Tang, *Sustainable Energy Technol. Assess.*, 2023, **60**, 103552.
6 C. Zhao, J. Ren, L. Lei, F. Liao, X. Shi, D. Zhou, K. Liu and Y. Zhao, *Appl. Phys. Lett.*, 2021, **119**, 223901.
7 C. Zhao, J. Ren, L. Lei, F. Liao, K. Liu and Y. Zhao, *Appl. Phys. Lett.*, 2022, **121**, 123906.
8 X. Hu, S. Luo, J. Leng, C. Wang, Y. Chen, J. Chen, X. Li and H. Zeng, *Sci. Adv.*, 2023, **9**, eadh5081.
9 Z. Lin, S. Lv, Z. Yang, J. Qiu and S. Zhou, *Adv. Sci.*, 2022, **9**, 2102439.
10 Y. Wang, W. Zhao, Y. Guo, W. Hu, C. Peng, L. Li, Y. Wei, Z. Wu, W. Xu, X. Li, Y. D. Suh, X. Liu and W. Huang, *Light: Sci. Appl.*, 2023, **12**, 155.
11 L. Lian, M. Zheng, W. Zhang, L. Yin, X. Du, P. Zhang, X. Zhang, J. Gao, D. Zhang, L. Gao, G. Niu, H. Song, R. Chen, X. Lan, J. Tang and J. Zhang, *Adv. Sci.*, 2020, **7**, 2000195.
12 M. Li, Y. Wang, L. Yang, Z. Chai, Y. Wang and S. Wang, *Angew. Chem., Int. Ed.*, 2022, **61**, e202208440.
13 D. Yang, L. Li, S. Liu, X. Hu, X. Zhang, Z. Xu, S. Guo, B. Wang, X. Tang, Z. Chen, X. Li, Q. Xu and H. Zeng, *Inorg. Chem. Front.*, 2024, DOI: **10.1039/d4qi01274g**.
14 R. Lin, Y. Zhu, L. Chen, W. Zheng, M. Xu, J. Ruan, R. Li, T. Li, Z. Lin, L. Cheng, Y. Ding, F. Huang and X. Ouyang, *PhotoniX*, 2022, **3**, 9.
15 W. Wang, H. Qi, F. Liu, H. Meng, J. Cai, S. Xu, S. Jing, F. Hong, Y. Zhu, H. Xu, R. Xu, J. Lai, F. Xu and L. Wang, *Crys. Growth Des.*, 2020, **20**, 3474–3481.
16 M. Chen, L. Sun, X. Ou, H. Yang, X. Liu, H. Dong, W. Hu and X. Duan, *Adv. Mater.*, 2021, **33**, 2104749.
17 N. Yasui, T. Kobayashi, Y. Ohashi and T. Den, *J. Cryst. Growth*, 2014, **399**, 7–12.
18 Y. Zhou, J. Chen, O. M. Bakr and O. F. Mohammed, *ACS Energy Lett.*, 2021, **6**, 739–768.
19 X. Ouyang, R. Lin, Y. Ding, Y. Liang, W. Zheng, L. Chen, X. Song, F. Huang and X. Ouyang, *Mater. Chem. Front.*, 2021, **5**, 4739–4745.
20 X. Li, J. Chen, D. Yang, X. Chen, D. Geng, L. Jiang, Y. Wu, C. Meng and H. Zeng, *Nat. Commun.*, 2021, **12**, 3879.
21 Y. Ding, R. Lin, Y. Liang, W. Zheng, L. Chen, X. Ouyang, X. Ouyang and F. Huang, *J. Phys. Chem. Lett.*, 2021, **12**, 7342–7349.
22 Z. Xu, X. Tang, Y. Liu, Z. Zhang, W. Chen, K. Liu and Z. Yuan, *ACS Appl. Mater. Interfaces*, 2019, **11**, 14191–14199.
23 W. Chen, X. Tang, Y. Liu, Z. Xu, Y. Zicheng, Z. Zhang and K. Liu, *Int. J. Energy Res.*, 2019, **43**, 4520–4533.
24 J.-X. Wang, X. Wang, J. Yin, L. Gutiérrez-Arzaluz, T. He, C. Chen, Y. Han, Y. Zhang, O. M. Bakr, M. Eddaoudi and O. F. Mohammed, *ACS Energy Lett.*, 2022, **7**, 10–16.
25 Y. Wang, M. Li, Z. Chai, Y. Wang and S. Wang, *Angew. Chem., Int. Ed.*, 2023, **62**, e202304638.
26 Y. Li, B. Liu, L. Chen, S. He, J. Liu, X. Wang, N. Zhao, L. Zhou, W. Shu and X. Ouyang, *J. Mater. Chem. C*, 2023, **11**, 12759–12763.
27 R. Lin, Y. Ding, W. Zheng, M. Jin, L. Chen, X. Ouyang and F. Huang, *Cell Rep. Phys. Sci.*, 2021, **2**, 100437.
28 H. Shankar, W. W. Yu, Y. Kang and P. Kar, *Sci. Rep.*, 2022, **12**, 7848.
29 C.-Y. Huang, C. Zou, C. Mao, K. L. Corp, Y.-C. Yao, Y.-J. Lee, C. W. Schlenker, A. K. Y. Jen and L. Y. Lin, *ACS Photonics*, 2017, **4**, 2281–2289.
30 D. Yang, X. Zhang, Y. Yang, Z. Xu, S. Liu, K. Cheng, S. Guo, Q. Xu, S. Jeon, L. Li and H. Zeng, *ACS Materials Lett.*, 2024, **6**, 1439–1446.

31 J. Shi, W. Ge, J. Zhu, M. Saruyama and T. Teranishi, *ACS Appl. Nano Mater.*, 2020, **3**, 7563–7571.
32 C. Wang, Y. Zhang, A. Wang, Q. Wang, H. Tang, W. Shen, Z. Li and Z. Deng, *Chem. Mater.*, 2017, **29**, 2157–2166.
33 Y. Tan, Y. Zou, L. Wu, Q. Huang, D. Yang, M. Chen, M. Ban, C. Wu, T. Wu, S. Bai, T. Song, Q. Zhang and B. Sun, *ACS Appl. Mater. Interfaces*, 2018, **10**, 3784–3792.
34 H. Wang, N. Sui, X. Bai, Y. Zhang, Q. Rice, F. J. Seo, Q. Zhang, V. L. Colvin and W. W. Yu, *J. Phys. Chem. Lett.*, 2018, **9**, 4166–4173.
35 D. Yang, Z. Xu, C. Gong, L. Su, X. Li, X. Tang, D. Geng, C. Meng, F. Xu and H. Zeng, *J. Mater. Chem. A*, 2021, **9**, 8772–8781.
36 Y. Wang, J. Ren, X. Zhou and G. Zhang, *Mater. Chem. Front.*, 2023, **7**, 2175–2207.
37 S. Liang, M. Zhang, G. M. Biesold, W. Choi, Y. He, Z. Li, D. Shen and Z. Lin, *Adv. Mater.*, 2021, **33**, 2005888.
38 W. Chen, M. Zhou, Y. Liu, X. Yu, C. Pi, Z. Yang, H. Zhang, Z. Liu, T. Wang, J. Qiu, S. F. Yu, Y. (Michael) Yang and X. Xu, *Adv. Funct. Mater.*, 2022, **32**, 2107424.
39 Y. Wang, J. He, H. Chen, J. Chen, R. Zhu, P. Ma, A. Towers, Y. Lin, A. J. Gesquiere, S. Wu and Y. Dong, *Adv. Mater.*, 2016, **28**, 10710–10717.
40 Q. Zhou, Z. Bai, W. Lu, Y. Wang, B. Zou and H. Zhong, *Adv. Mater.*, 2016, **28**, 9163–9168.
41 Y. Liu, T. Chen, Z. Jin, M. Li, D. Zhang, L. Duan, Z. Zhao and C. Wang, *Nat. Commun.*, 2022, **13**, 1338.
42 H. Teng, L. Ma, C. Cui, Z. Li, K. Chen, X. Ming, Y. Guo, Q. Zhang, Z. Ge, Y. Cheng, A. Pan and Y. Zhang, *ACS Appl. Mater. Interfaces*, 2024, **16**, 23924–23931.
43 L. Wang, K. Fu, R. Sun, H. Lian, X. Hu and Y. Zhang, *Nano-Micro Lett.*, 2019, **11**, 52.
44 F. Di Stasio, S. Christodoulou, N. Huo and G. Konstantatos, *Chem. Mater.*, 2017, **29**, 7663–7667.
45 S. Liu, X. Liu, Y. Wu, D. Zhang, Y. Wu, H. Tian, Z. Zheng and W.-H. Zhu, *Matter*, 2022, **5**, 2319–2333.
46 N. T.-H. Pham, *Polymers*, 2021, **13**, 2352.
47 C. Chen, X. Wang, Z. Li, X. Du, Z. Shao, X. Sun, D. Liu, C. Gao, L. Hao, Q. Zhao, B. Zhang, G. Cui and S. Pang, *Angew. Chem., Int. Ed.*, 2022, **61**, e202113932.
48 Y. Wu, J. Chen, D. Zheng, X. Xia, S. Yang, Y. Yang, J. Chen, T. Pullerits, K. Han and B. Yang, *J. Phys. Chem. Lett.*, 2022, **13**, 5794–5800.
49 Q. Zhang, Z. Li, M. Liu, L. Kong, W. Zheng, B. Wang and L. Li, *J. Phys. Chem. Lett.*, 2020, **11**, 993–999.
50 M. Liu, Q. Wan, H. Wang, F. Carulli, X. Sun, W. Zheng, L. Kong, Q. Zhang, C. Zhang, Q. Zhang, S. Brovelli and L. Li, *Nat. Photonics*, 2021, **15**, 379–385.
51 S. Huang, C. Bian, W. Xu, H. Zhang, S. Gao, Y. Wang and Y. Wang, *Phys. Chem. Chem. Phys.*, 2024, **26**, 3578–3586.
52 Y. He, Z. Xu, H. Wang, M. Bian, Y. Liu and X. Tang, *J. Lumin.*, 2023, **255**, 119600.
53 Z. Xu, Y. Liu and X. Tang, *Adv. Astronaut. Sci. Technol.*, 2020, **3**, 125–131.
54 R. J. Schott, C. L. Weaver, M. A. Prelas, K. Oh, J. B. Rothenberger, R. V. Tompson and D. A. Wisniewski, *Nucl. Technol.*, 2013, **181**, 349–353.
55 Y. Zhang, R. Sun, X. Ou, K. Fu, Q. Chen, Y. Ding, L.-J. Xu, L. Liu, Y. Han, A. V. Malko, X. Liu, H. Yang, O. M. Bakr, H. Liu and O. F. Mohammed, *ACS Nano*, 2019, **13**, 2520–2525.
56 H. Wei, Y. Fang, P. Mulligan, W. Chuirazzi, H.-H. Fang, C. Wang, B. R. Ecker, Y. Gao, M. A. Loi, L. Cao and J. Huang, *Nat. Photonics*, 2016, **10**, 333–339.